

Single Microphone Own Voice Detection based on Simulated Transfer Functions for Hearing Aids

Mathuranathan Mayuravaani, W. Bastiaan Kleijn, Andrew Lensen, Charlotte Sørensen

Abstract—This paper presents a simulation-based approach to own voice detection (OVD) in hearing aids using a single microphone. While OVD can significantly improve user comfort and speech intelligibility, existing solutions often rely on multiple microphones or additional sensors, increasing device complexity and cost. To enable ML-based OVD without requiring costly transfer-function measurements, we propose a data augmentation strategy based on simulated acoustic transfer functions (ATFs) that expose the model to a wide range of spatial propagation conditions. A transformer-based classifier is first trained on analytically generated ATFs and then progressively fine-tuned using numerically simulated ATFs, transitioning from a rigid-sphere model to a detailed head-and-torso representation. This hierarchical adaptation enabled the model to refine its spatial understanding while maintaining generalization. Experimental results show 95.52% accuracy on simulated head-and-torso test data. Under short-duration conditions, the model maintained 90.02% accuracy with one-second utterances. On real hearing aid recordings, the model achieved 80% accuracy without fine-tuning, aided by lightweight test-time feature compensation. This highlights the model’s ability to generalize from simulated to real-world conditions, demonstrating practical viability and pointing toward a promising direction for future hearing aid design.

Index Terms—own voice detection, hearing instruments, machine learning, signal processing, speech processing.

I. INTRODUCTION

HEARING AIDS play a crucial role in improving the quality of life for individuals with hearing impairments by amplifying speech. However, a common complaint among hearing aid users is that their own voice sounds excessively loud or unnatural when using the device [1]. To mitigate this issue, hearing care professionals often reduce amplification levels to enhance comfort. However, this reduction compromises speech clarity and audibility, making communication more difficult [2]. Developing a robust method for efficiently identifying the wearer’s own voice is crucial, as it enables personalized adjustments to maintain both comfort and intelligibility [3].

Although many modern hearing aids are equipped with multiple microphones, there are several practical motivations for pursuing reliable single microphone Own Voice Detection (OVD). Multi-microphone processing increases hardware cost, power consumption, and calibration complexity, which can limit applicability in low-cost or entry-level devices [4]. In addition, Some users rely on a single device due to unilateral hearing loss or personal preference. Even in multi-microphone systems, microphone signals may be temporarily unavailable or degraded due to occlusion, wind noise, or power-saving

modes [5], making a single microphone solution a valuable fallback. For these reasons, single microphone OVD remains a practically important and complementary alternative to multi-microphone solutions.

The majority of existing OVD methods rely on traditional signal processing techniques, such as cross-correlation, adaptive filtering, and beamforming [6]–[9]. These methods typically require multiple microphones and complex directional filtering, which increases hardware costs and makes them unsuitable for individuals with single-ear hearing loss. Machine learning (ML) approaches, often applied in single microphone configurations, have gained popularity in speaker identification and distance estimation tasks [10]–[13], as they can capture complex patterns in speech signals, improving adaptability and accuracy. However, existing ML-based methods primarily focus on the vocal characteristics of the users, which typically require more processing time to be recognized.

This work proposes a spatial-analysis-based approach for single microphone OVD in hearing aids by leveraging differences in acoustic propagation paths between the user’s own voice and external speakers. Instead of relying solely on speaker-dependent vocal characteristics, we use acoustic transfer functions (ATFs) to model the distinct propagation paths of own voice and external speech as they reach the hearing aid microphone, and we train a data-driven classifier to learn discriminative spatial-spectral patterns from ATF-augmented speech.

To overcome the practical difficulty of collecting large-scale measured ATFs across anatomies and device configurations, we propose a two-stage simulation-based ATF generation pipeline that progressively increases geometric realism. We first generate analytically derived ATFs based on simplified geometries to cover a wide range of spatial configurations, enabling scalable data generation with controlled variation. We then generate numerically simulated ATFs using finite-element modeling, transitioning from a rigid sphere to a detailed head-and-torso model. These ATFs are used to augment speech signals for training and progressively fine-tuning the OVD classifier. We formulate OVD as segment-level binary classification problem and use a transformer-based classifier to aggregate frame-level features into a single decision. The main contribution of this work is demonstrating that spatial cues embedded via simulated ATFs can enable effective single microphone OVD, validated on real hearing aid recordings. We emphasize that this study focuses on offline segment-level detection as a feasibility analysis, and causal streaming implementation with low-latency inference is left for future work.

II. BACKGROUND

OVD has been a longstanding challenge in speech processing, particularly for hearing aids. Early approaches relied on classical signal processing techniques, later evolving to incorporate multichannel methods and, more recently, ML-based solutions. One of the earliest OVD methods was proposed by Rasmussen et al. [8], who used a cross-correlation technique to exploit the symmetrical positioning of the user’s mouth. Their method aimed to detect speech originating from the median plane. To improve near-field detection, they introduced the mouth-to-random-far-field (M2R) technique; however, if a straight-ahead external speaker is close enough, their voice may also exhibit near-field characteristics, posing a challenge for accurate differentiation. Another classical approach involved adaptive filtering, as proposed by Merks et al. [6], where two microphones were used to estimate a transfer function for OVD. While effective in some cases, this method was susceptible to errors in the presence of strong external speech sources. Bone-conductive sensors have also been explored [6], [14], but their effectiveness is limited by low signal-to-noise ratio (SNR) and the need for direct skull contact.

Hoang et al. [15] applied beamforming and relative acoustic transfer functions (RATFs) for interfering speech suppression. They considered the ATF from the user’s mouth to the microphones to be approximately time-invariant. With the microphones positioned close to the user’s mouth, the own voice signal can be significantly louder than both the target and interfering speech signals, especially at lower frequencies when the own voice is active. However, these considerations may not apply to a speaker facing directly forward or with varying loudness. A steep slope in the frequency response of the rear microphones in a head-mounted array was observed, attributed to diffraction and the directional propagation of own voice [16]. A similar effect is also present in our free-space ATFs, where the frequency response exhibits a continuous steep slope with increasing frequency (see section III-A).

ML-based OVD methods have also been explored. Pohlhausen et al. [17] proposed a binaural OVD method utilizing near-ear microphones and a random forest classifier, distinguishing own voice from external sounds based on phase and amplitude symmetry. Similarly, Pertilä et al. [18] developed an LSTM-based online OVD system for in-ear devices using multiple microphones and accelerometers which increase system complexity and cost. Lopez-Espejo et al. [19], [20] trained a deep residual network for OVD within a keyword spotting system, leveraging measured head-related transfer functions (HRTFs) and own voice transfer functions (OVTFs) from a hearing assistive device. However, these methods rely on measured, device-specific transfer functions which limits the coverage of transfer functions. In particular, expanding transfer function measurements to capture the full range of acoustic paths across anatomies and device configurations remains challenging, motivating simulation-based ATF generation as a scalable alternative for training OVD models. Additionally, distance-based ML approaches for speaker separation have been investigated using single-channel audio [11], [13].

Acoustic modeling has played a significant role in under-

standing voice propagation and directivity patterns. Various analytical models [21], [22] have been employed to study speech and singing sound propagation, often utilizing simplified representations of the human head. Many of these models approximate the acoustic effects of the head and mouth using geometrical shapes, such as spheres. For instance, Blandin et al. [21] analyzed the directivity patterns around the head, assuming a vibrating plane piston model set within an infinite baffle. Their work aimed to enhance the quality of artistic performances in concert halls by investigating the influence of the mouth opening size on voice directivity, comparing both measurements and simulations. They observed that the overall features of the radiated sound could be predicted from the properties of the vibrating piston. Similarly, the impact of mouth configuration and torso shape on voice directivity was explored during singing [22]. Utilizing both piston and spherical cap models for their simulations, they found that significant changes in the mouth opening size considerably affect voice directivity. In our approach, we present a model that represents the human head as a rigid sphere with the mouth modeled as a vibrating cap on its surface, providing a physically grounded approach to detecting the wearer’s own voice in a hearing aid. A point source is represented as an external speaker, allowing us to analyze how sound scatters from the rigid sphere. By jointly modeling both the wearer’s voice and external sources, we capture the spatial propagation differences that distinguish them, allowing us to generate ATFs that enable us to augment the speech data for training ML algorithm.

While previous works have applied ML for OVD and utilized transfer functions in speech modeling, to the best of our knowledge, no study has incorporated analytical and numerical ATFs for augmenting training data in ML-based OVD using only a single microphone. In this work, we propose a novel data augmentation strategy that enhances training data diversity using synthetic ATF-augmented speech, and we evaluate a conformer encoder-based classifier [23] for segment-level own voice versus external speaker classification. The conformer architecture provides a flexible mechanism for aggregating frame-level speech features into a single decision, improving robustness to phonetic variability while operating in a single microphone setting.

III. METHOD

In this study, our objective is to classify the hearing aid wearer’s own voice versus external speakers’ voices. To achieve this, we employ an ML algorithm to perform the classification. Since ML models require large and diverse training datasets to generalize effectively, we augment the speech data using ATFs. Specifically, we generate training samples using both analytically derived ATFs, which introduce controlled variability, and numerically simulated ATFs, which incorporate detailed human anatomy for more realistic spatial representations. The model was first trained on analytically augmented data and subsequently fine-tuned using samples generated from numerical simulations.

To construct these ATFs for data augmentation and analysis, we model the wearer’s head as a rigid sphere that captures

scattering effects shaping the acoustic paths to the hearing aid microphone. External speech is modeled as radiation from a point source scattered by the rigid sphere, whereas own voice is modeled as radiation from a vibrating spherical cap on the same sphere, representing mouth radiation coupled with head scattering. In both cases, the resulting pressure is evaluated at the hearing aid microphone location on the sphere surface. The same source definitions are used in the numerical simulations, while the geometry is progressively refined from a rigid sphere to detailed head and head-and-torso models to increase anatomical realism. Similar geometric approximations, such as spherical caps and pistons, have been used in previous studies [21], [22], [24] to model sound radiation and head-related scattering.

Section III-A presents the fundamental equations governing the considered geometries. Section III-B details the analytical approach for modeling sound propagation. We validate this approach by comparing analytical results with numerical simulations and also generate ATFs using simulation software, as discussed in Section III-C. Finally, the OVD algorithm is described in Section III-D.

A. Geometry and basic formulas

We consider a point source with a volume velocity \tilde{U}_0 located at a distance d from a rigid sphere of radius R (Figure 1) to model the effect of an external speaker's voice reaching a hearing aid user. Our goal is to determine the pressure field $\tilde{p}(r, \theta)$ at an observation point on the sphere, corresponding to the ear location of the hearing aid user. $r_1 = \sqrt{r^2 + d^2 - 2rd \cos \theta}$ is the distance from the point source to the observation point. In spherical coordinates, the incident pressure field due to the point source is [25], [26]:

$$\tilde{p}(r, \theta) = jk\rho_0 c \tilde{U}_0 \frac{e^{-jk r_1}}{4\pi r_1}. \quad (1)$$

where j is the imaginary unit, k is the wave number, ρ_0 is density of air and c is speed of propagation of the sound wave.

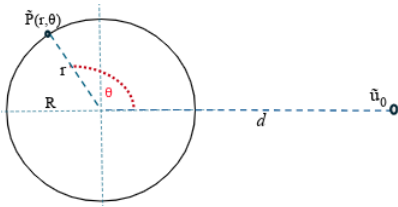


Fig. 1: Geometry of point source and rigid sphere.

This expression describes the free-field pressure at an arbitrary location before considering reflections and scattering. This expression can be expanded to account for the interaction with the sphere in terms of spherical Bessel functions j_n and Legendre functions P_n as follows:

$$\tilde{p}_I(r, \theta) = \frac{k^2 \rho_0 c \tilde{U}_0}{4\pi} \sum_{n=0}^{\infty} (2n+1) h_n^{(2)}(kd) j_n(kr) P_n(\cos \theta), \quad r \leq d. \quad (2)$$

When an external speaker's voice reaches the hearing aid user, part of the sound is scattered by the head. The scattered pressure field is given by:

$$\tilde{p}_s(r, \theta) = -\frac{k^2 \rho_0 c \tilde{U}_0}{4\pi} \sum_{n=0}^{\infty} (2n+1) h_n^{(2)}(kd) \frac{j_n'(kR)}{h_n^{(2)'(kR)} h_n^{(2)}(kr)} P_n(\cos \theta). \quad (3)$$

The total pressure field at the observation point is obtained by summing the incident and scattered fields:

$$\tilde{p}(r, \theta) = \tilde{p}_I(r, \theta) + \tilde{p}_s(r, \theta). \quad (4)$$

This total pressure field is critical for analyzing how an external speaker's voice propagates to the hearing aid user. In contrast to an external speaker, the hearing aid user's own voice originates from the mouth and propagates differently. To model this, we represent the mouth as a vibrating spherical cap on a rigid sphere that vibrates with an axial velocity of \tilde{u}_0 (Figure 4) [25], [27]. The near-field pressure due to the oscillating cap can be derived, which describes how the user's own voice propagates before interacting with the hearing aid. This pressure field is given by [28]:

$$\tilde{p}(r, \theta) = -jk\rho_0 c \tilde{u}_0 \left(\frac{\sin^2 \alpha}{4h_0^{(2)'(kR)}} h_0^{(2)}(kR) + \frac{1 - \cos^3 \alpha}{2h_1^{(2)'(kR)}} h_1^{(2)}(kr) \cos \theta - \sin \alpha \sum_{n=2}^{\infty} (2n+1) \frac{\sin \alpha P_n(\cos \alpha) + \cos \alpha P_n^1(\cos \alpha)}{2(n-1)(n+2)h_n^{(2)'(kR)}} h_n^{(2)}(kr) P_n(\cos \theta) \right). \quad (5)$$

where α is the half-angle of the arc formed by the cap.

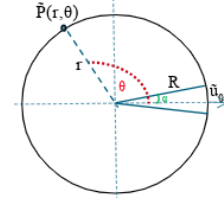


Fig. 4: Geometry of oscillating cap in a rigid sphere.

A comparison of directivity patterns at 5 kHz is presented in Figure 5, considering a point source scattering from a rigid sphere, and a vibrating spherical cap on the sphere for 5 kHz. The results show a significant difference in the relative sound pressure level (SPL) changes with respect to the on-axis direction. As the frequency increases, the pressure at the ear location decreases, resulting in a steeper slope for the head-shaped radius in the context of vibrating cap scattering from a rigid sphere.

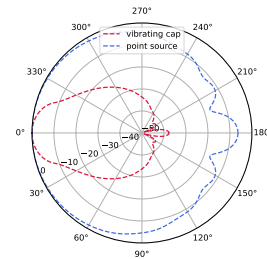


Fig. 5: Directivity pattern $20 \log_{10}(D(\theta)/D(0))$ of the near-field pressure for a straight-ahead point source scattering from a 7 cm rigid sphere and a spherical cap ($\alpha = 20^\circ$).

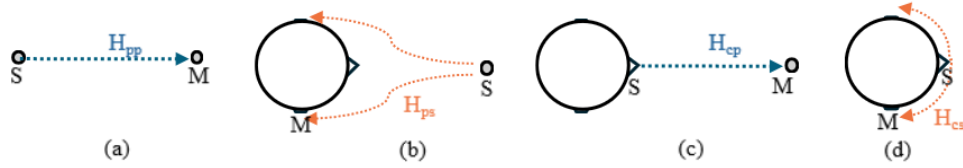


Fig. 2: Mapping the pressure between (a) a point source and a point receiver, (b) a point source and a rigid sphere, (c) a rigid sphere source with vibrating cap and a point receiver, and (d) vibrating spherical cap and location on the rigid sphere. Here, S denotes the source location and M denotes the receiver (microphone) location.

B. Analytical Modelling Approach

This section describes how analytically derived ATFs are computed and applied to generate synthetic hearing aid microphone signals. We consider two classes: (i) external speaker and (ii) own voice. The two classes differ in the assumed geometry model and propagation path: external speech is modeled as radiation from a point source scattered by a rigid sphere, whereas own voice is modeled as radiation from a vibrating spherical cap mounted on the same sphere. The resulting ATFs characterize the frequency-domain mapping from the source model to the hearing aid microphone position and are subsequently used to generate ATF-augmented speech samples for ML training (described in Section III-D).

Let $P_{out_r}(k)$ denote the complex pressure spectrum at a reference microphone receiver location (used as a known observation in the simulation pipeline). Our objective is to generate the pressure spectrum at the hearing aid location, denoted by $P_{f_other}(k)$ and $P_{f_own}(k)$, for both external and own voice conditions. We define the following frequency-domain transfer functions parameterized by the acoustic wavenumber $k = \omega/c$ (see figure 2):

- $H_{pp}(k)$: ATF from a point source to a point receiver.
- $H_{ps}(k)$: ATF from a point source to a receiver location on the rigid sphere.
- $H_{cp}(k)$: ATF from a vibrating spherical-cap source (own voice model) to a point receiver.
- $H_{cs}(k)$: ATF from a vibrating spherical-cap source to a receiver location on the rigid sphere.

For the external-speaker class, the speech waveform is assumed to radiate from a point source. The pressure at the reference receiver $P_{out_r}(k)$ is first mapped back to an estimate of the source pressure using the inverse ATF $H_{pp}^{-1}(k)$, and then forward-propagated to the hearing aid microphone position using $H_{ps}(k)$ (see Fig. 3(a)):

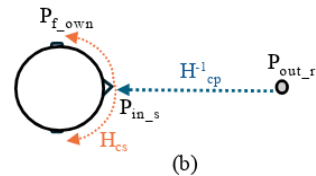
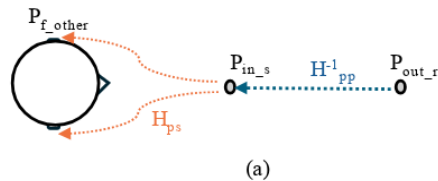


Fig. 3: Mapping the pressure at an angle on the sphere when (a) a speech signal is from a point source from a distance (external speaker) and (b) a speech signal is from a vibrating cap on the rigid sphere (own voice).

$$P_{f_other}(k) = H_{ps}(k) H_{pp}^{-1}(k) P_{out_r}(k). \quad (6)$$

For the own voice class, the speech waveform is assumed to radiate from a vibrating spherical cap mounted on a rigid sphere, representing sound radiation from the wearer's mouth. The reference observation is mapped to an equivalent cap-source spectrum using $H_{cp}^{-1}(k)$ and then propagated to the hearing aid microphone using $H_{cs}(k)$ (see figure 3(b)):

$$P_{f_own}(k) = H_{cs}(k) H_{cp}^{-1}(k) P_{out_r}(k). \quad (7)$$

These ATFs (see figure 6(a)) enable the simulation of how speech propagates to the hearing aid user.

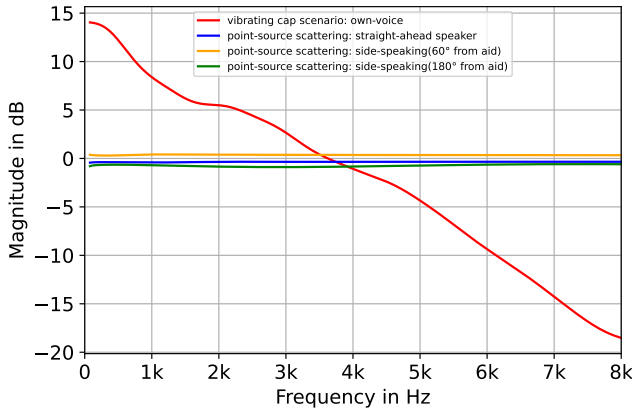
1) $H_{pp}(k)$: The ATF models free-field propagation from a point source to a point receiver (Fig. 2(a)). It is defined as

$$H_{pp}(k) = \frac{r_0 e^{-jkr_1}}{r_1 e^{-jkr_0}}. \quad (8)$$

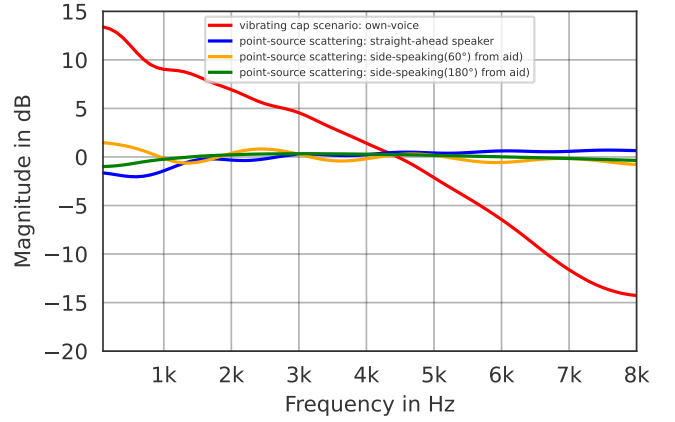
Here, r_0 is a near-field reference distance (close to the source) and r_1 is the source-to-receiver distance. We use $H_{pp}^{-1}(k)$ to map the reference pressure back to the equivalent source location.

2) $H_{ps}(k)$: The ATF models propagation from a point source to a receiver location on a rigid sphere/head model (Fig. 2(b)), capturing scattering effects at the sphere surface. It is expressed as

$$H_{ps}(k) = \frac{\sum_{n=0}^{\infty} (2n+1) h_n^{(2)}(kd) \left(j_n(kR) - \frac{j_n'(kR)}{h_n^{(2)'(kR)}} h_n^{(2)}(kR) \right) P_n(\cos \theta)}{\sum_{n=0}^{\infty} (2n+1) h_n^{(2)}(kd) j_n(kr) P_n(\cos \theta)}. \quad (9)$$



(a) Analytical results.



(b) Simulation results.

Fig. 6: Comparison between analytical and numerical simulation results of ATF with rigid sphere.

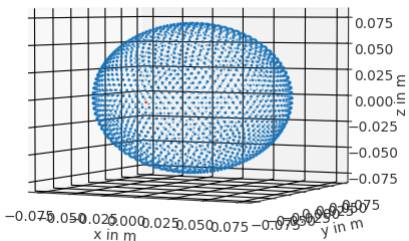
3) $H_{cp}(k)$: The ATF models propagation from a vibrating spherical-cap source mounted on a rigid sphere to a point receiver (Fig. 2(c)). It is given by

$$H_{cp}(k) = \frac{\left(\frac{\sin^2 \alpha}{4h_0^{(2)}(kR)} h_0^{(2)}(kr_1) + \frac{1-\cos^3 \alpha}{2h_1^{(2)}(kR)} h_1^{(2)}(kr_1) - \sin \alpha \right)}{\left(\frac{\sin^2 \alpha}{4h_0^{(2)}(kR)} h_0^{(2)}(kr_0) + \frac{1-\cos^3 \alpha}{2h_1^{(2)}(kR)} h_1^{(2)}(kr_0) - \sin \alpha \right)} \cdot \frac{\sum_{n=2}^{\infty} (2n+1) \frac{\sin \alpha P_n(\cos \alpha) + \cos \alpha P_n^1(\cos \alpha)}{2(n-1)(n+2)h_n^{(2)}(kR)} h_n^{(2)}(kr_1)}{\sum_{n=2}^{\infty} (2n+1) \frac{\sin \alpha P_n(\cos \alpha) + \cos \alpha P_n^1(\cos \alpha)}{2(n-1)(n+2)h_n^{(2)}(kR)} h_n^{(2)}(kr_0)}. \quad (10)$$

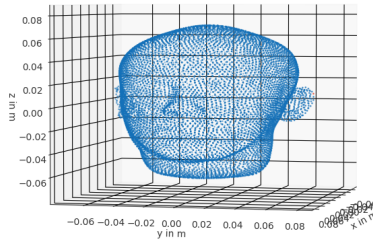
We use $H_{cp}^{-1}(k)$ to estimate the equivalent spherical-cap source spectrum from the reference observation.

4) $H_{cs}(k)$: The ATF models propagation from a vibrating spherical-cap source to a receiver location on the rigid sphere/head model (Fig. 2(d)), representing how own voice is observed at the hearing aid microphone. It is expressed as

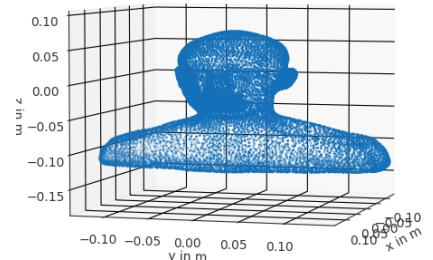
$$H_{cs}(k) = \frac{\left(\frac{\sin^2 \alpha}{4h_0^{(2)}(kR)} h_0^{(2)}(kR) + \frac{1-\cos^3 \alpha}{2h_1^{(2)}(kR)} h_1^{(2)}(kR) \cos \theta - \sin \alpha \right)}{\left(\frac{\sin^2 \alpha}{4h_0^{(2)}(kR)} h_0^{(2)}(kR) + \frac{1-\cos^3 \alpha}{2h_1^{(2)}(kR)} h_1^{(2)}(kR) - \sin \alpha \right)} \cdot \frac{\sum_{n=2}^{\infty} (2n+1) \frac{\sin \alpha P_n(\cos \alpha) + \cos \alpha P_n^1(\cos \alpha)}{2(n-1)(n+2)h_n^{(2)}(kR)} h_n^{(2)}(kR) P_n(\cos \theta)}{\sum_{n=2}^{\infty} (2n+1) \frac{\sin \alpha P_n(\cos \alpha) + \cos \alpha P_n^1(\cos \alpha)}{2(n-1)(n+2)h_n^{(2)}(kR)} h_n^{(2)}(kR)}. \quad (11)$$



(a) 3D Rigid sphere model.



(b) 3D Human head model.



(c) 3D Human head-and-torso model.

Fig. 7: 3D model meshes created in Blender for simulation.

C. Numerical Modelling Approach

We used *Mesh2HRTF* [29], [30], an open-source software package for the numerical calculation of HRTFs to generate ATFs from 3D mesh models. We utilized its implementation of the multilevel fast multipole method (ML-FMM-BEM), a combination of the multilevel fast multipole method (ML-FMM) [31] and boundary element method (BEM) [32]. The 3D model meshes of rigid sphere (see Fig. 7(a)) and human models (see Fig. 7(b), (c)) were created using Blender [33] and post-processed using MeshInspector [34].

The rigid sphere mesh enables direct comparison with our analytical model and provides a foundational step for progressively fine-tuning the model toward more anatomically realistic head and torso representations. In *Mesh2HRTF*, radiation from vibrating elements was used to model the vibrating cap for the rigid sphere and the human mouth for human models, while the other speaker was represented as a point source. The source code for inspecting SOFA files was modified, and customized evaluation grids were generated to suit our specific requirements. The simulation scenarios for other speakers and own voice were generated as illustrated in Figures 3(a) and 3(b), respectively. The figure 6 presents a comparison between analytical and numerical simulation results for rigid sphere models, highlighting their alignment.

The ATFs were generated for three models of increasing anatomical complexity: a rigid sphere, a human head, and a head-and-torso configuration. These ATFs account for varia-

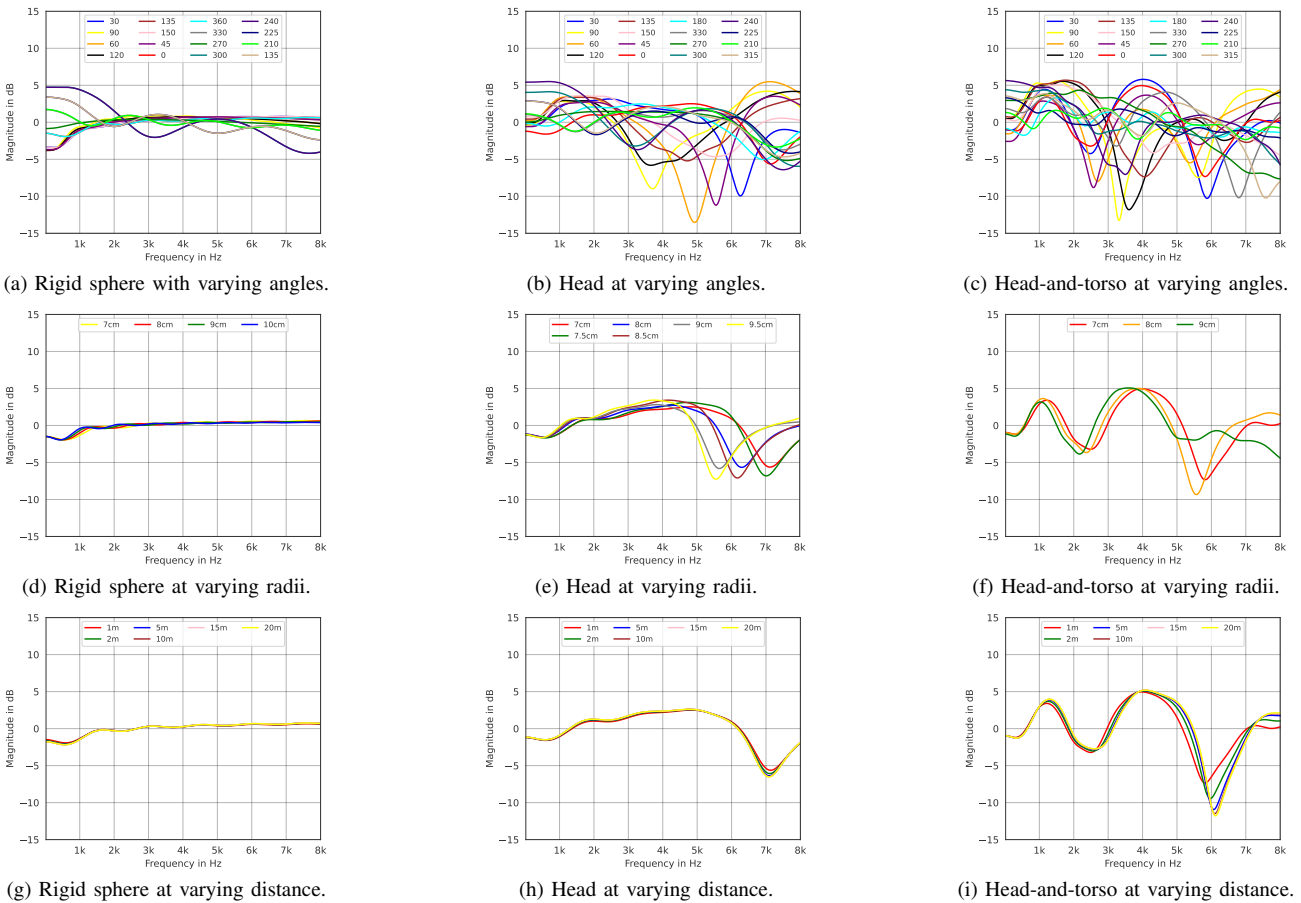


Fig. 8: ATFs for external speaker scenarios: (a)–(c) show a 3D model with a 7 cm head radius and a point source positioned 1 m away from various angles. (d)–(f) illustrate a 3D model with varying head radii and a point source positioned 1 m straight ahead. (g)–(i) depict a 3D model with a 7 cm head radius and a point source at varying distances.

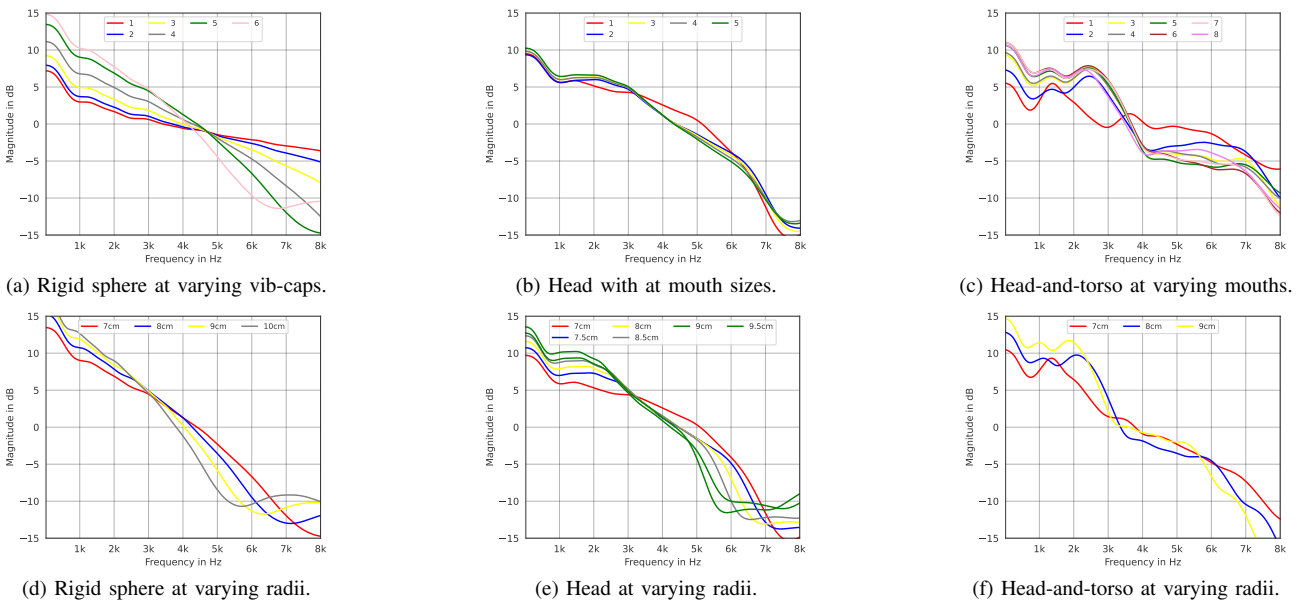


Fig. 9: ATFs for own voice scenarios: (a)–(c) show a 3D model with a 7 cm head radius, with varying mouth angles, where the number indicates increasing angles. (d)–(f) illustrate a 3D model with varying head radii.

TABLE I: Description of the ATF dataset. (*) indicates the number of variations considered for each parameter.

Model	Angles	Head radius	Distance	Mouth angle	Ear location	Total ATF	Own voice	Other speaker
Analytical approach								
Rigid sphere	0°-360° (360)	7cm-10cm (50)	0.5m-20m (100)	5°-20° (15)	90°-120° (20)	153516	76757	76759
Numerical approach								
Rigid sphere	0°-360° (18)	7cm-10cm (4)	1m-20m (39)	(6)	90°	2544	48	2496
Human head	0°-360° (18)	7cm-9.5cm (6)	1m-20m (24)	(5)	90°	2414	110	2304
Head & torso	0°-360° (18)	7cm-9cm (3)	0.5m-20m (25)	(8)	90°	2904	336	2568

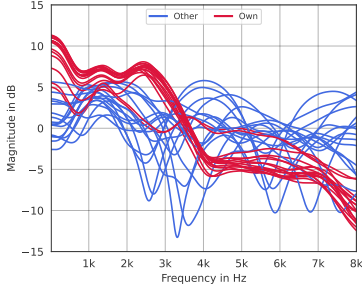


Fig. 10: Comparison of ATFs between own voice and various angles of external speakers’ voice (head & torso).

tions in speaker angles, distances, and anatomical dimensions. In addition, ATFs were generated for elevation angles of $+5^\circ$ and -5° in different models to account for slight vertical speaker offsets. Figure 8 summarizes the ATFs for external speaker scenarios. Subplots (a)–(c) demonstrate how directional angle influences ATFs across models, with the rigid sphere showing smoother responses and the head-and-torso model exhibiting stronger spectral notches and directional dependence especially above 3 kHz. Subplots (d)–(f) highlight the impact of changing head radius, where increases in head size lead to more pronounced high-frequency attenuation, particularly evident in the human head and head-and-torso cases. Subplots (g)–(i) show that increasing distance reduces fluctuation strength in the ATF, though structural model differences persist.

Figure 9 focuses on the ATFs for the own voice condition. Unlike external sources, these responses exhibit a steep spectral slope, particularly in the head-and-torso model, indicating strong near-field characteristics and spatial filtering. Furthermore, Figure 10 directly compares ATFs of own voice and external speakers using the head-and-torso model. This comparison further underscores that own voice ATFs maintain

steep spectral slopes with relatively consistent patterns, while external speaker ATFs show greater angular variability and flatter responses.

D. Own voice detection algorithm

We apply transfer functions derived from both analytical and numerical simulation models to a clean speech wave in order to replicate how a hearing aid user perceives incoming sound. To incorporate these ATFs into the speech, we first extract the Short-Time Fourier Transform (STFT) from raw audio data, and the extracted STFT is then modified by applying the ATFs, simulating how sound propagates to the hearing aid user’s ear. Following this, log-mel spectrogram is derived from the transformed STFT and used as input to the classifier.

We formulate OVD as a segment-level binary classification task, where each input segment is assigned a single label (own voice or external speaker). We adopt a transformer-based model with temporal gate pooling [35], which aggregates frame-level features across the segment into a single decision. This temporal aggregation improves robustness to phonetic variability and short-term spectral fluctuations while leveraging spatial-spectral cues embedded by the ATFs. We emphasize that the present work evaluates offline segment-level classification.

IV. EXPERIMENTAL SETUP

In this section, we describe the dataset used for training and evaluation, the model architecture and hyperparameters, and the fine-tuning strategies employed.

A. Dataset

VoxCeleb1 dataset [36] was used as the source of clean speech waveforms for generating ATF-augmented training data. The dataset contains 153516 utterances, which are randomly assigned to the own voice or external speaker class (50% each) prior to ATF-based transformations. The ATF dataset was generated using both analytically derived ATFs and numerically simulated ATFs. Each ATF class (external-speaker and own-voice) was split into training (70%), validation (10%), and testing (20%), ensuring that ATFs used during testing are not seen during training. The detailed ATF configuration parameters and dataset sizes are provided in Table I, and the dataset split is summarized in Table II. For each speech utterance, an ATF is randomly sampled from

TABLE II: Distribution of ATF dataset into training, validation, and testing sets for classes 0 (Other) and 1 (Own).

ATF Dataset	Training		Validation		Testing	
	1	0	1	0	1	0
Rigid sphere (Analytical)	69180	69181	3452	3452	4125	4126
Rigid sphere (Numerical)	33	1744	5	250	10	490
Head model (Numerical)	77	1612	11	231	22	461
Head & torso (Numerical)	235	1797	33	257	68	514

the corresponding split and applied to generate the ATF-augmented waveform.

To assess noise robustness, the MUSAN dataset [37], which includes a diverse set of noises such as music, speech, and ambient sounds, was used to augment the training data by adding background noise at various SNR levels (0, 5, 10, 15, and 20 dB). To assess generalization to unseen speech content and speakers, we evaluate the model on LibriSpeech [38], which is not used during training. OVD test samples are generated by applying the same ATF augmentation procedure using held-out ATFs from the test split. The resulting LibriSpeech test set contains 4,125 utterances per class.

We also included real-world recordings from a hearing aid prototype to assess the model’s robustness in practical acoustic environments. Three participants provided informed consent prior to data collection. The recordings were made using two prototype units of the same hearing aid device design connected to a Mackie ProFX16 audio mixer in a controlled acoustic room. For the own voice condition, the participant wore the device and read pre-defined sentences to ensure consistent speech content. For the external-speaker condition, the participant continued wearing the device while a second person spoke in the same room, thereby representing external speech in a realistic conversational scenario. In addition to this, we also collected recordings using a loudspeaker playback setup. The estimated SNR of the recorded signals was approximately 23 dB. For evaluation, we extracted 250 one-second segments, evenly distributed between the two classes. A disjoint subset of 50 segments was used for calibration to estimate statistics for domain-adaptation compensation, while the remaining segments were used exclusively for testing.

A distribution mismatch arises when testing on real hearing aid data as the model was trained on simulated ATF-augmented speech. To mitigate this mismatch, we apply a lightweight test-time feature compensation. Let X denote the log-Mel spectrogram extracted from a real speech segment. Device-dependent spectral coloration introduced by the hearing aid [39] is first compensated using a white-noise reference recording, yielding $\tilde{X} = X - \mu_W$, where μ_W is the mean log-Mel spectrum of recorded white noise. To align the feature distribution with the simulated training domain, we apply a lightweight test-time statistic matching step inspired by correlation-alignment approaches in unsupervised domain adaptation (e.g., CORAL [40]). Specifically,

$$X' = (\tilde{X} - \mu_R) \odot \frac{\sigma_S}{\sigma_R} + \mu_S. \quad (12)$$

where μ_R and σ_R are the per-frequency mean and standard deviation estimated from a disjoint calibration subset of the evaluation data, and μ_S and σ_S are the corresponding statistics estimated from the simulated training data. The operator \odot denotes element-wise multiplication. This compensation is applied only during inference and does not require any model fine-tuning.

In addition to real-world recordings, we evaluate the proposed approach on a publicly available measured-ATF hearing aid dataset [19]. In this dataset, clean speech signals from the Google Speech Commands dataset [41] are convolved with

ATFs measured from a hearing aid worn by a human subject, yielding both own-voice and external-speaker conditions. Although the dataset provides multi-microphone recordings, only the front-microphone channel is used to match the single microphone setting considered in this work.

B. Model

We followed the standard training approach from [35], which employs a conformer-based encoder [23], and reduced the number of parameters (0.9M) to optimize computational efficiency while maintaining classification performance. The model is configured with a hidden size of 128, a feedforward hidden size of 512, 4 attention heads, and a single encoder layer. These modifications reduce computational complexity while maintaining classification performance. In preprocessing, raw audio data of 16000 Hz sample rate is segmented into fixed 15-second segments. The STFT is computed using a 25 ms window with a 10 ms stride, and an 80-channel log-mel spectrogram is used as input for the ML model.

C. Training methodology

The model was trained using a progressive adaptation training strategy [42], where the dataset complexity gradually increases to improve its performance in OVD. This approach follows a structured, multi-phase training process:

- 1) Training with analytical ATFs: Establishes a foundational understanding of sound propagation characteristics by allowing a wider range of parameter variations, including angles, distances, and head radii. For training, an AdamW optimizer with a learning rate of $1e-4$ and a linear-warmup-and-cosine-decay scheduler were employed, conducting training across a maximum of 50 epochs with a batch size of 64.
- 2) Fine-tuning with numerical ATFs: The model is fine-tuned using simulated ATFs, progressively transitioning from a rigid sphere model \rightarrow human head model \rightarrow head-and-torso model, allowing it to incrementally adapt to more complex practical application. Each fine-tuning stage was run for 5 epochs. We employed two distinct fine-tuning strategies: (1) fine-tuning only the last classification layer and (2) fine-tuning both the feed-forward and classification layers [43].

To assess robustness under noisy conditions, the model was trained using simulated speech data mixed with noise. Specifically, 70% of the training data consisted of clean speech, while the remaining 30% was randomly mixed with noise samples from the MUSAN dataset [37] at varying SNR levels of 0, 5, 10, 15, and 20 dB.

V. RESULTS

In this section, we present and analyze the experimental results. The OVD task is formulated as segment-level binary classification, where each speech segment is assigned a single label (own voice vs. external speaker). VoxCeleb1 contains variable-length utterances; during training we use the full available utterance duration up to a maximum of 15 s to

TABLE III: Test accuracy (%) of models fine-tuned with different ATF configurations, using two fine-tuning strategies: (i) last classification layer only, and (ii) feed-forward layers with the classification layer. Evaluation was conducted on the Head-and-torso ATF dataset using utterances with a maximum length of 15 seconds.

Model fine-tuned on	Test Accuracy (%) on Head & Torso ATF dataset		
	Last Layer Fine-Tuned	Fine-Tuned	Feed-Forward + Last Layer Fine-Tuned
+ Sphere ATF	83.78 \pm 0.24		91.46 \pm 0.20
+ Head ATF	90.54 \pm 0.30		93.40 \pm 0.19
+ Head & torso ATF	91.04 \pm 0.18		95.52 \pm 0.20

expose the model to diverse phonetic content. The adopted conformer encoder supports variable-length inputs via padding or cropping and attention masking, and produces frame-level embeddings that are aggregated using temporal gate pooling to obtain a single segment-level prediction. At test time, we additionally evaluate the same trained model on shorter one-second segments to assess robustness under lower-latency conditions and to approximate practical real-world usage scenarios.

A. Training and progressive fine-tuning

The model trained solely on analytically simulated ATFs already demonstrated strong generalization to simulation-based test sets, achieving 86% accuracy on the head-and-torso dataset without any fine-tuning. Table III presents the test accuracy for each stage of fine-tuning. Testing was performed on the head-and-torso ATF dataset, and the test set includes variable-length utterances up to 15 seconds. When fine-tuning only the final classification layer with numerically simulated ATFs from the same sphere geometry, accuracy dropped slightly to 83.78%, likely due to domain shift between analytical and numerical ATFs. This indicates that updating only the classifier is insufficient to bridge the gap between different modeling approaches. Progressively fine-tuning the classification layer alone with head-and-torso ATFs improved the accuracy to 91.04%, surpassing the original baseline. However, fine-tuning both the feed-forward and classification layers led to a substantial performance gain, achieving 95.52% accuracy on the same dataset. These findings highlight the importance of internal feature representations in adapting to complex spatial conditions, and indicate that limiting fine-

tuning to the classification layer constrains the model’s generalization capacity. Table IV shows the test accuracy of models evaluated on one-second utterances. The final fine-tuned model achieved an accuracy of 90.02% on the head-and-torso ATF dataset.

B. Noise augmentation

To further assess the robustness of the proposed model, we trained it with background noise augmentation using the MUSAN dataset. Table V reports the test accuracy across different noise types (Noise, Music, and Speech) and SNRs. The model shows reasonable resilience to noise, with performance decreasing gradually as SNR decreases. Furthermore, to assess generalization, we tested the model on the LibriSpeech dataset with added noise, a dataset not seen during training, and observed consistently high performance across all SNR levels. These results confirm the model’s ability to generalize well across datasets and remain robust in diverse acoustic conditions. All evaluations were conducted on the Mesh2HRTF head-and-torso ATF test set using one-second utterances.

C. Real-world evaluation

We evaluated the proposed method on real-world recordings captured with a hearing aid prototype to assess robustness under practical acoustic and device conditions. The evaluation was performed on non-overlapping one-second segments. Training on simulated ATF-augmented speech introduces a distribution mismatch when evaluating real hearing aid recordings. To mitigate this mismatch, we applied a lightweight test-time feature compensation (Eq. 12) prior to inference, which subtracts pre-computed vectors from calibration test set representing hearing aid spectral coloration and simulation-to-real feature shifts. This procedure enables inference on real data without requiring any model fine-tuning.

The model fine-tuned on simulated head-and-torso ATFs achieved 90.02% accuracy on the corresponding simulated test set. When evaluated on the real-world recordings using compensation, the model attained 80.00% accuracy, demonstrating effective simulation-to-real transfer despite the absence of real-data fine-tuning. Finally, we report an oracle upper bound using class-conditional compensation, where ground-truth labels are used to select class-specific compensation vectors. This oracle setting achieves 86.50% accuracy and

TABLE IV: Test accuracy (%) across different fine-tuning stages and ATF datasets, demonstrating generalization performance. The first section of the table reports results from the model trained on the analytical ATF dataset and tested on all ATF datasets. The second section presents results after progressive fine-tuning of both the feed-forward and classification layers. All models were evaluated using one-second utterances.

Model	Test Accuracy (%)			
	Analytical ATFs	Rigid Sphere (Mesh)	Head Model (Mesh)	Head & Torso (Mesh)
Training on analytical ATFs				
Baseline (Analytical ATFs) (50 epochs)	89.59 \pm 0.14	83.69 \pm 0.25	86.43 \pm 0.15	85.12 \pm 0.14
Feed-Forward + classification layer fine-tuning on numerical simulation ATFs				
+ Fine-Tuned on Rigid Sphere (5 epochs)	-	84.42 \pm 0.27	88.74 \pm 0.08	86.87 \pm 0.19
+ Fine-Tuned on Head Model (5 epochs)	-	-	92.61 \pm 0.17	88.51 \pm 0.17
+ Fine-Tuned on Head & Torso (5 epochs)	-	-	-	90.02 \pm 0.29

TABLE V: Robustness to different noise types and SNR levels. Test accuracy (%) of the model trained on VoxCeleb1 with MUSAN noise augmentation, evaluated on both VoxCeleb1 and LibriSpeech using one-second utterances. The test ATF set is based on the Mesh2HRTF head-and-torso configuration.

Noise Type	SNR (dB)	VoxCeleb1	LibriSpeech
Noise	0	75.86 \pm 0.55	73.24 \pm 0.49
	5	77.88 \pm 0.34	75.55 \pm 0.53
	10	79.45 \pm 0.42	77.10 \pm 0.57
	15	80.70 \pm 0.35	78.28 \pm 0.51
	20	82.30 \pm 0.39	79.62 \pm 0.49
	30	85.69 \pm 0.16	82.79 \pm 0.38
Music	0	71.07 \pm 0.36	68.53 \pm 0.42
	5	74.26 \pm 0.21	71.70 \pm 0.47
	10	77.62 \pm 0.18	74.91 \pm 0.37
	15	81.00 \pm 0.28	77.67 \pm 0.30
	20	83.69 \pm 0.26	80.37 \pm 0.45
	30	87.96 \pm 0.15	84.83 \pm 0.46
Speech	0	81.23 \pm 0.24	75.46 \pm 0.39
	5	84.19 \pm 0.30	78.73 \pm 0.27
	10	86.59 \pm 0.33	81.62 \pm 0.27
	15	88.41 \pm 0.23	83.89 \pm 0.49
	20	89.65 \pm 0.09	85.67 \pm 0.38
	30	90.67 \pm 0.13	87.93 \pm 0.33

is reported only as an upper bound, as it relies on ground-truth labels. We note that the real-world validation is limited in scale and device. These results highlight that the proposed ATF-based simulation pipeline can produce models that generalize reasonably to real hearing aid recordings. To further characterize performance, Figure 11 shows ROC curves for both the simulated test set and the real hearing aid recordings. The simulated test set achieved an AUC of 0.96. On real recordings, label-free test-time compensation achieved an AUC of 0.80; for reference, the oracle class-specific compensation yields an AUC of 0.92 and serves as an upper bound real-data performance. Overall, these results demonstrate real-world validation of the proposed method.

D. Baseline comparison and measured-ATF evaluation

To provide a direct baseline comparison, we compare our method with the ResNet-based single microphone own voice detection model proposed by López-Espejo et al. [19]. We follow the same dataset splits [41] and evaluation protocol as in [19], and adopt matching optimization settings where applicable. We report class-conditional accuracies (own-voice and external-speaker subsets), overall accuracy, and model

TABLE VI: Effect of training data and adaptation strategy on own-voice/external-speaker detection performance using measured ATFs. Results are shown for the ResNet baseline trained on measured ATFs following [19] and for the proposed conformer-small model pretrained on analytical ATFs and fine-tuned on the same measured ATF dataset.

Training strategy	#ATF variations	Accuracy (%) on measured-ATF		
		Own	External	Overall
Measured-only (ResNet [19])	49 (measured)	97.52	80.18	93.15
Analytical \rightarrow Measured (5-ep FT, Conformer-small, ours)	17,966 (analytical) \rightarrow 49 (measured)	98.77	89.94	96.46

parameter counts to ensure a fair and transparent comparison.

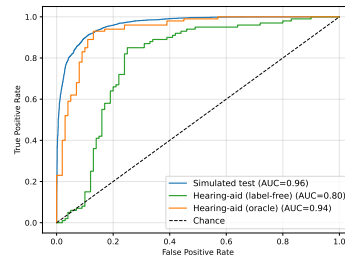


Fig. 11: ROC curves for simulated and real test data.

Table VII compares the two architectures under a controlled setting, where both models are trained and evaluated on the same simulated-ATF Google Speech Commands data generated using our ATF pipeline (17,966 analytically simulated ATF variations). To ensure a fair comparison, the proposed conformer is reduced to a smaller configuration and evaluated on one-second input segments to match the conditions of the ResNet baseline. The results show that the conformer-small achieves comparable own voice detection performance while providing substantially improved external-speaker and overall accuracy relative to the ResNet model. We note that the overall accuracy is influenced by class imbalance, with a larger proportion of own voice samples, consistent with the evaluation protocol in [19]. Table VI illustrates the impact of training data diversity and adaptation strategy. Pretraining on a large set of analytically simulated ATFs, followed by brief fine-tuning on the same measured ATFs used in [19] substantially improves external-speaker and overall accuracy compared to training on measured ATFs alone.

TABLE VII: Own-voice/external-speaker detection performance on simulated-ATF Google Speech Commands [41]. Both models use the same dataset split and 17,966 analytical ATFs, and are sequentially fine-tuned up to the head-and-torso ATF stage.

Model	#Params	Accuracy (%) on head-and-torso ATF		
		Own	External	Overall
ResNet [19]	238k	98.24	83.18	94.30
Conformer-small (ours)	307k	98.38	91.80	96.66

E. Analysis of acoustic features for OVD

While previous results demonstrate the model’s robustness, it remains important to understand the acoustic features the model relies on for OVD. In particular, loudness differences

between the wearer’s voice and external speakers could be a simple cue that the model might exploit. To investigate this, we conducted experiments where the amplitude of the external speaker’s audio was artificially increased to simulate closer proximity. Despite these modifications, the model’s detection accuracy remained largely unchanged, achieving 89.90% for the fine-tuned model on the head-and-torso dataset. These results indicate that the model does not rely solely on amplitude cues but instead leverages spatial acoustic features to discriminate between own voice and other speakers. This is crucial for real-world use, where speaker volume may vary significantly due to differences in speaking style or environment.

Additionally, repeating the one-second utterance to fill the 15-second input window did not improve accuracy compared to zero-padding, indicating the model does not benefit from redundant temporal information. Finally, an ablation study where the ATF input was removed during testing resulted in a substantial drop in accuracy to 49.67%, confirming that spatial cues are critical for the classification.

VI. CONCLUSION

This study presents a simulation-based training framework for single microphone OVD in hearing aids. A conformer-based classifier was first trained on analytically derived ATFs to expose the model to a wide range of spatial configurations, and subsequently fine-tuned using numerically simulated ATFs with increasing anatomical realism. Unlike prior approaches that rely on multi-microphone arrays, speaker-dependent cues, or costly transfer-function measurements, the proposed method leverages simulated spatial propagation cues to distinguish own voice from external speakers. The model achieved 95.52% accuracy on simulated head-and-torso test data using full-length utterances and maintained 90.02% accuracy on one-second segments, demonstrating robustness to shorter input durations. On real hearing aid recordings, the model achieved 80.50% accuracy after feature compensation without fine-tuning. Although this real-world validation is limited in scale, it provides an initial feasibility demonstration that models trained on simulated ATFs can generalize to real hearing aid recordings. A controlled baseline comparison on a measured-ATF benchmark further shows that the proposed approach achieves performance comparable to a ResNet-based single microphone OVD baseline, while benefiting from simulation-based pretraining. Future work will focus on reducing model complexity, improving detection accuracy for shorter temporal windows, and enabling causal real-time operation suitable for deployment on hearing aid hardware.

ACKNOWLEDGMENTS

Funding for this work was provided by GN Store Nord A/S.

REFERENCES

- [1] M. Froehlich, T. Powers, E. Branda, and J. Weber, “Perception of own voice wearing hearing aids: Why “natural” is the new normal,” *Audiology Online*, 2018.
- [2] E. H. Høydal, “A new own voice processing system for optimizing communication,” *Hearing Review*, vol. 24, no. 11, pp. 20–22, 2017.
- [3] J. Hengen, I. L. Hammarström, and S. Stenfelt, “Perception of one’s own voice after hearing-aid fitting for naive hearing-aid users and hearing-aid refitting for experienced hearing-aid users,” *Trends in hearing*, vol. 24, p. 2331216520932467, 2020.
- [4] J. M. Kates, *Hearing Aids*. Springer, 2008.
- [5] K. Chung, “Challenges and recent developments in hearing aids: Part i. speech understanding in noise, microphone technologies and noise reduction algorithms,” *Trends in amplification*, vol. 8, no. 3, pp. 83–124, 2004.
- [6] I. Merks, “Hearing assistance system with own voice detection,” *Acoustical Society of America Journal*, vol. 135, no. 1, p. 573, 2014.
- [7] O. Al-hazaimeh, S. A. Alomari, J. Alsakran, and N. Alhindawi, “Cross correlation–new based technique for speaker recognition,” *Int J Acad Res*, vol. 6, pp. 232–239, 2014.
- [8] K. B. Rasmussen and S. Laugesen, “Method for detection of own voice activity in a communication device,” Mar. 31 2009, uS Patent 7,512,245.
- [9] M. Zohourian, G. Enzner, and R. Martin, “Binaural speaker localization integrated into an adaptive beamformer for hearing aids,” *IEEE/ACM Transactions on Audio, Speech, and Language Processing*, vol. 26, no. 3, pp. 515–528, 2017.
- [10] J. Wang, H. Liu, L. Xu, W. Yang, W. Yi, and F. Liu, “Lightweight target speaker separation network based on joint training,” *EURASIP Journal on Audio, Speech, and Music Processing*, vol. 2023, no. 1, p. 53, 2023.
- [11] K. Patterson, K. Wilson, S. Wisdom, and J. R. Hershey, “Distance-based sound separation,” *arXiv preprint arXiv:2207.00562*, 2022.
- [12] D. Wang, X. Xiao, N. Kanda, T. Yoshioka, and J. Wu, “Target speaker voice activity detection with transformers and its integration with end-to-end neural diarization,” in *ICASSP 2023-2023 IEEE International Conference on Acoustics, Speech and Signal Processing (ICASSP)*. IEEE, 2023, pp. 1–5.
- [13] M. Neri, A. Politis, D. Krause, M. Carli, and T. Virtanen, “Speaker distance estimation in enclosures from single-channel audio,” *IEEE/ACM Transactions on Audio, Speech, and Language Processing*, 2024.
- [14] Y.-L. Wei, B. Islam, R. RAJAGOPALAN, and romit choudhury, “Self-supervised speech enhancement using multi-modal data,” 2023. [Online]. Available: https://openreview.net/forum?id=OqPD_6kukm
- [15] P. Hoang, J. M. De Haan, Z.-H. Tan, and J. Jensen, “Multichannel speech enhancement with own voice-based interfering speech suppression for hearing assistive devices,” *IEEE/ACM Transactions on Audio, Speech, and Language Processing*, vol. 30, pp. 706–720, 2022.
- [16] K. Kazama, T. Nakashima, and N. Ono, “Measurement of relative transfer function for own voice in head-mounted microphone array,” in *2024 Asia Pacific Signal and Information Processing Association Annual Summit and Conference (APSIPA ASC)*. IEEE, 2024, pp. 1–5.
- [17] J. Pohlhausen, I. Holube, and J. Bitzer, “Near-ear sound pressure level distribution in everyday life considering the user’s own voice and privacy,” *Acta Acustica*, vol. 6, p. 40, 2022.
- [18] P. Pertilä, E. Fagerlund, A. Huttunen, and V. Myllylä, “Online own voice detection for a multi-channel multi-sensor in-ear device,” *IEEE Sensors Journal*, vol. 21, no. 24, pp. 27 686–27 697, 2021.
- [19] I. López-Espejo, Z.-H. Tan, and J. Jensen, “Keyword spotting for hearing assistive devices robust to external speakers,” *arXiv preprint arXiv:1906.09417*, 2019.
- [20] López-Espejo, Iván and Tan, Zheng-Hua and Jensen, Jesper, “Improved external speaker-robust keyword spotting for hearing assistive devices,” *IEEE/ACM Transactions on Audio, Speech, and Language Processing*, vol. 28, pp. 1233–1247, 2020.
- [21] R. Blandin and M. Brandner, *Influence of the vocal tract on voice directivity*. Universitätsbibliothek der RWTH Aachen, 2019.
- [22] M. Brandner, R. Blandin, M. Frank, and A. Sontacchi, “A pilot study on the influence of mouth configuration and torso on singing voice directivity,” *The Journal of the Acoustical Society of America*, vol. 148, no. 3, pp. 1169–1180, 2020.
- [23] A. Gulati, J. Qin, C.-C. Chiu, N. Parmar, Y. Zhang, J. Yu, W. Han, S. Wang, Z. Zhang, Y. Wu *et al.*, “Conformer: Convolution-augmented transformer for speech recognition,” *arXiv preprint arXiv:2005.08100*, 2020.
- [24] R. M. Aarts and A. J. Janssen, “Comparing sound radiation from a loudspeaker with that from a flexible spherical cap on a rigid sphere,” *Journal of the Audio Engineering Society*, vol. 59, no. 4, pp. 201–212, 2011.
- [25] L. Beranek and T. Mellow, *Acoustics: sound fields, transducers and vibration*. Academic Press, 2019.
- [26] “Spherical Wave Scattering by a Rigid Sphere,” http://ansol.us/Products/Coustyx/Validation/MultiDomain/Scattering/SphericalWave/HardSphere/Downloads/dataset_description.pdf, accessed: 2024-02-04.

- [27] R. M. Aarts and A. J. Janssen, "Sound radiation from a resilient spherical cap on a rigid sphere," *The Journal of the Acoustical Society of America*, vol. 127, no. 4, pp. 2262–2273, 2010.
- [28] L. L. Beranek and T. Mellow, *Acoustics: sound fields and transducers*. Academic Press, 2012.
- [29] H. Ziegelwanger, W. Kreuzer, and P. Majdak, "Mesh2hrtf: Open-source software package for the numerical calculation of head-related transfer functions," in *22nd international congress on sound and vibration*, 2015.
- [30] W. Kreuzer, K. Pollack, P. Majdak, and F. Brinkmann, "Mesh2hrtf/numcalc: An open-source project to calculate hrdfs and wave scattering in 3d," in *Proceedings of the Euroregio BNAM Joint Acoustics Conference*, 2022, pp. 443–452.
- [31] Z.-S. Chen, H. Waubke, and W. Kreuzer, "A formulation of the fast multipole boundary element method (fmbem) for acoustic radiation and scattering from three-dimensional structures," *Journal of Computational Acoustics*, vol. 16, no. 02, pp. 303–320, 2008.
- [32] L. Gaul, M. Kögl, and M. Wagner, *Boundary element methods for engineers and scientists: an introductory course with advanced topics*. Springer Science & Business Media, 2013.
- [33] B. Foundation, "Blender: 3d creation suite," accessed: [01 February 2023]. [Online]. Available: <https://www.blender.org>
- [34] MeshInspector Team, "Meshinspector," 2025, accessed: Jan 02, 2025. [Online]. Available: <https://meshinspector.com/>
- [35] H. Kawano and S. Shimizu, "An effective transformer-based contextual model and temporal gate pooling for speaker identification," *arXiv preprint arXiv:2308.11241*, 2023.
- [36] A. Nagrani, J. S. Chung, and A. Zisserman, "Voxceleb: a large-scale speaker identification dataset," *arXiv preprint arXiv:1706.08612*, 2017.
- [37] D. Snyder, G. Chen, and D. Povey, "Musan: A music, speech, and noise corpus," *arXiv preprint arXiv:1510.08484*, 2015.
- [38] V. Panayotov, G. Chen, D. Povey, and S. Khudanpur, "Librispeech: an asr corpus based on public domain audio books," in *2015 IEEE international conference on acoustics, speech and signal processing (ICASSP)*. IEEE, 2015, pp. 5206–5210.
- [39] J. M. Kates, *Digital Hearing Aids*. Plural Publishing, 2008.
- [40] B. Sun and K. Saenko, "Deep coral: Correlation alignment for deep domain adaptation," in *European conference on computer vision*. Springer, 2016, pp. 443–450.
- [41] P. Warden, "Speech commands: A dataset for limited-vocabulary speech recognition," *arXiv preprint arXiv:1804.03209*, 2018.
- [42] Y. Bengio, J. Louradour, R. Collobert, and J. Weston, "Curriculum learning," in *Proceedings of the 26th annual international conference on machine learning*, 2009, pp. 41–48.
- [43] A. Barcovschi, R. Jain, and P. Corcoran, "A comparative analysis between conformer-transducer, whisper, and wav2vec2 for improving the child speech recognition," in *2023 International Conference on Speech Technology and Human-Computer Dialogue (SpeD)*. IEEE, 2023, pp. 42–47.

VII. BIOGRAPHY SECTION

Mathuranathan Mayuravaani is currently pursuing a Ph.D. degree in the School of Engineering and Computer Science at Victoria University of Wellington, New Zealand. Her research interests include speech signal processing and machine learning.

Andrew Lensen is a Senior Lecturer and Programme Director of Artificial Intelligence at Victoria University of Wellington, New Zealand. He holds a B.Sc.(Hons) and a Ph.D. degree (2019) from Victoria University of Wellington. His current research interests include explainable AI, interdisciplinary applications of AI, and the societal impacts of AI use in New Zealand. He is a Senior Member of the IEEE (2025).

Charlotte Sørensen is a Research Scientist at GN ReSound, Denmark. She received the B.S. and M.Sc. degrees in Biomedical Engineering and Informatics, and the Ph.D. degree, from Aalborg University, Denmark. Her research interests include speech signal processing with emphasis on speech intelligibility prediction, measurement of speech intelligibility, and speech enhancement for hearing aid applications.

W. Bastiaan Kleijn is Professor at Victoria University of Wellington, New Zealand (since 2010) and a research scientist at Google (since 2011). He was a professor at TU Delft (2011-2021) and KTH Stockholm (1996-2014) and prior to that a Member of Technical Staff in the Research Division of AT&T Bell Laboratories. He holds a PhD in Soil Science and an MSc in Physics from the University of California, Riverside, an MSEE from Stanford University, and a PhD in Electrical Engineering from TU Delft. He is Fellow of the IEEE (1999), the Royal Society of New Zealand (2021), and Engineering New Zealand (2024).